# Differential ionization of a one-electron target under bare-ion impact: Application to proton-impact ionization of atomic hydrogen

H. R. J. Walters[1] and Colm T. Whelan[2]

[1]*Centre for Theoretical Atomic, Molecular, and Optical Physics, School of Mathematics and Physics, Queen's University, Belfast BT7 1NN, United Kingdom*

[2]*Department of Physics, Old Dominion University, Norfolk, Virginia 23529-0116, USA*

(Received 21 October 2015; published 21 December 2015)

A single-center coupled pseudostate approximation originally used by McGovern *et al.* [Phys. Rev. A **79**, 042707 (2009)] to study differential ionization under ion impact is extended to take account of electron exchange. The approximation is fully quantal and includes the interaction between the projectile and target nuclei as well as post-collisional interactions between the ionized electron and the two nuclei. Calculations are presented for proton-impact ionization of atomic hydrogen at 75 keV. These include fully (triple) differential cross sections which illustrate how the post-collisional interaction switches from being dominated by the interaction between the ejected electron and the target nucleus to being dominated by the electron interaction with the projectile nucleus (charge exchange to the continuum). Comparison is made with some measurements of the double differential cross section with respect to ejected electron energy and proton scattering angle. While overall agreement between theory and the experimental data is encouraging, detailed agreement is lacking. The need for more experimental work is emphasized.

DOI: 10.1103/PhysRevA.92.062712 PACS number(s): 34.50.Fa, 52.20.Hv

## I. INTRODUCTION

To fully understand ionization dynamics it is essential to study it at the differential level. To guide theoretical understanding the availability of suitable experimental measurements is important. For heavy particle impact such measurements, of increasing sophistication, have recently become available, e.g., [1–20]. Most useful are fully differential measurements [11–20]. Mostly the target has been He or something heavier [5,8–10,20]. But with such targets understanding the dynamics is further complicated by not having exact target wave functions. Ideally, the target is H for which exact analytic wave functions exist. While fully differential measurements have not yet been made for H, some very testing double differential data have recently appeared [18,19]. A number of different theoretical approximations have been matched against these data [19] but none have provided a completely satisfactory description.

Recently, we developed a powerful coupled pseudostate approximation to describe differential ionization under heavy particle impact [21–24]. This has been applied to ionization of He and Li by protons, $C^{6+}$, $O^{8+}$, $Au^{24+}$, and $Au^{53+}$ [25–28] at elevated impact energies. The approximation is designed for energies and geometries in which charge exchange is considered not to be important. Then, it is adequate to expand the system wave function in pseudostates centered on the target nucleus. However, with reducing impact energy it becomes essential to take explicit account of charge exchange channels. In particular, as far as ionization is concerned, we need to tackle the problem of charge exchange to the continuum [29,30] in which the ionized electron ends up asymptotically under the influence of the projectile rather than the target. It is our purpose here to extend the aforementioned pseudostate approximation to include explicit allowance for exchange. In this first step we restrict ourselves to a hydrogenic target and report results for ionization of H by protons [31] which, at the double differential level, can be compared with the measurements from [18,19].

Although semiclassical in appearance, it should be emphasized that the approximation we use is fully quantal. As shown in [21] it results from a quantal treatment in which the scattering angle is assumed to be very small and where the propagator $1/(k_\beta^2 - k^2 + i\epsilon)$ is replaced by $1/(2k_\beta(k_\beta - k_z) + i\epsilon)$, where the $z$ direction is the direction of incidence of the projectile. Both of these are very good approximations for heavy particle collisions at all but the lowest energies. In [19] Schulz *et al.* emphasized the importance of the PT interaction, i.e., the interaction between the projectile and target nuclei, and of the post-collisional interaction (PCI) between the electron and the ionized target and scattered projectile. Both are taken into account in our approximation. Indeed, the importance of the PT interaction was emphasized in the original version of the approximation described in [21–28]. There are three aspects to PCI. The first is when the ejected electron moves with a "low" velocity relative to the target. Ever since the work of Curran and Walters [32,33] on electron impact it has been clear that this is well taken into account by pseudostates on the target. This has been conclusively demonstrated again in our earlier studies of heavy particle collisions [21–28]. The second is when the ejected electron velocity is low relative to the scattered projectile ion, the so-called charge exchange to the continuum [29,30]. In the present approximation this is accommodated by the pseudostates on the projectile. The third aspect, when the ejected electron is equally affected by both the target and projectile ions, is more problematic and is a matter that comes under discussion in the present work.

We begin in Sec. II with the formulation of the coupled pseudostate theory, now with explicit inclusion of exchange. As in [21] we start with an impact parameter formulation, in Sec. II A, and then show its connection to the wave treatment (i.e., a quantal treatment), in Sec. II B. Next we consider the extraction of ionization data from the theory in Sec. II C, first for the total ionization cross section and then, for the main task of this paper, for fully differential ionization. Here we discuss an ambiguity in the theory and suggest two possible avenues

 

of attack, "coherent" and "incoherent." Results are presented in Sec. III for proton impact on atomic hydrogen at 75 keV, an energy at which about one-third of the total ionization cross section comes from charge exchange to the continuum, and therefore a good test of the new "with exchange" theory. First (Sec. III A), as a test of our computations, we show that we get good agreement with the earlier extensive work of Winter [34] on integrated cross sections, not only for ionization but also for discrete excitations. Next, in Sec. III B, we explore our results for fully (triple) differential cross sections, illustrating the transition between the case where the ejected electron is slow relative to the target ion to where it moves with the projectile, i.e., illustrating the changes in PCI. We also examine the differences between the "coherent" and "incoherent" approaches to differential ionization. Finally, in Sec. III C, we look at the double differential cross section $d^2\sigma^L/dEd\Omega_p$ and compare it to the data of [18,19]. Once more we are interested in how PCI changes and in the difference between "coherent" and "incoherent" cross sections. In Sec. IV we present our conclusions.

Throughout we use atomic units (a.u.) in which $\hbar = m_e = e = 1$. All reported differential cross sections refer to the laboratory frame of reference [21].

## II. THEORY

We consider a bare projectile ion of mass $M_P$ and charge $Z_P$ incident with velocity $\boldsymbol{v}_0$ upon a one-electron target of nuclear mass $M_T$ and nuclear charge $Z_T$ which is stationary in the laboratory. We first look at the time-dependent impact parameter treatment of this problem and then show how it is related to the wave treatment. This relationship shows, as before [21], that, although the time-dependent approach is often described as "semiclassical," when correctly interpreted it is a fully quantal approximation under the assumption that the projectile is scattered through a small angle and with small velocity change, which is indeed the case for heavy ionic projectiles at all but the very lowest energies.

### A. Impact parameter treatment

Let the projectile move along a straight line with constant velocity $\boldsymbol{v}_0$ and at impact parameter $\mathbf{b}$ relative to the target nucleus. Let $\mathbf{R}$ be the position vector of the projectile at time $t$ relative to the target nucleus and such that

$$\mathbf{R} = \mathbf{b} + \boldsymbol{v}_0 t. \tag{1}$$

Let $\mathbf{r}_T$ ($\mathbf{r}_P$) be the position vector of the electron relative to the target (projectile) nucleus. Then

$$\mathbf{r}_P = \mathbf{r}_T - \mathbf{R}. \tag{2}$$

The wave function $\Psi$ describing the dynamics of the electron satisfies the time-dependent Schrödinger equation

$$H\Psi = i\frac{\partial \Psi}{\partial t}, \tag{3}$$

where $\mathbf{r}_T$ and $t$ are independent variables. The Hamiltonian $H$ may be split as

$$H = H_T + V_T = H_P + V_P, \tag{4}$$

where

$$\begin{aligned} H_T &= -\frac{1}{2}\nabla_T^2 - \frac{Z_T}{r_T}, \\ V_T &= \left(\frac{Z_P Z_T}{R} - \frac{Z_P}{|\mathbf{R}-\mathbf{r}_T|}\right), \\ H_P &= -\frac{1}{2}\nabla_P^2 - \frac{Z_P}{r_P}, \\ V_P &= \left(\frac{Z_P Z_T}{R} - \frac{Z_T}{|\mathbf{R}+\mathbf{r}_P|}\right), \end{aligned} \tag{5}$$

with $\nabla_T^2$ ($\nabla_P^2$) being with respect to the coordinate $\mathbf{r}_T$ ($\mathbf{r}_P$). $H_T$ ($H_P$) is the Hamiltonian of the electron in the field of the target (projectile) nucleus. $V_T$ ($V_P$) is the interaction of the target (projectile) nucleus and electron with the projectile (target) nucleus.

The wave function $\Psi$ may be expanded as

$$\begin{aligned} \Psi = &\sum_{\alpha=1}^{N} a_\alpha(\mathbf{b},t) e^{-i\epsilon_\alpha t}\psi_\alpha(\mathbf{r}_T) \\ &+ \sum_{\beta=1}^{M} b_\beta(\mathbf{b},t) e^{-i\left(E_\beta + \frac{v_0^2}{2}\right)t}\phi_\beta(\mathbf{r}_P) e^{i\boldsymbol{v}_0\cdot\mathbf{r}_T}, \end{aligned} \tag{6}$$

where $\psi_\alpha(\mathbf{r}_T)$ ($\phi_\beta(\mathbf{r}_P)$) correspond to states of the electron about the target (projectile) nucleus of energy $\epsilon_\alpha$ ($E_\beta$). These states diagonalize $H_T$ and $H_P$ according to

$$\begin{aligned} \langle\psi_\alpha|H_T|\psi_{\alpha'}\rangle &= \epsilon_\alpha\delta_{\alpha\alpha'}, \quad \langle\psi_\alpha|\psi_{\alpha'}\rangle = \delta_{\alpha\alpha'}, \\ \langle\phi_\beta|H_P|\phi_{\beta'}\rangle &= E_\beta\delta_{\beta\beta'}, \quad \langle\phi_\beta|\phi_{\beta'}\rangle = \delta_{\beta\beta'}, \end{aligned} \tag{7}$$

and, in general, are a mixture of eigenstates and pseudostates. Substituting (6) into (3) and forming the scalar product with each $\psi_\alpha(\mathbf{r}_T)$ and each $e^{i\boldsymbol{v}_0\cdot\mathbf{r}_T}\phi_\beta(\mathbf{r}_P)$ leads to the coupled equations

$$i\mathbf{S}\frac{d\mathbf{A}}{dt} = \mathbf{F}\mathbf{A}, \tag{8}$$

where

$$\mathbf{A} \equiv \begin{pmatrix} a_1 \\ \cdot \\ \cdot \\ \cdot \\ a_N \\ b_1 \\ \cdot \\ \cdot \\ \cdot \\ b_M \end{pmatrix}, \tag{9}$$

$$\mathbf{S} \equiv \begin{pmatrix} \mathbf{I} & \mathbf{S_{12}} \\ \mathbf{S}_{12}^\dagger & \mathbf{I} \end{pmatrix}, \tag{10}$$

$$(\mathbf{S}_{12})_{\alpha\beta} = e^{i\left(\epsilon_\alpha - E_\beta - \frac{v_0^2}{2}\right)t}\langle\psi_\alpha(\mathbf{r}_T)|\phi_\beta(\mathbf{r}_P)e^{i\boldsymbol{v}_0\cdot\mathbf{r}_T}\rangle, \tag{11}$$

$$\mathbf{F} \equiv \begin{pmatrix} \mathbf{F_{11}} & \mathbf{F_{12}} \\ \mathbf{F}_{21} & \mathbf{F}_{22} \end{pmatrix}, \tag{12}$$

$$(\mathbf{F}_{11})_{\alpha\alpha'} = e^{i(\epsilon_\alpha - \epsilon_{\alpha'})t}\langle\psi_\alpha(\mathbf{r}_T)|V_T|\psi_{\alpha'}(\mathbf{r}_T)\rangle, \tag{13}$$

$$(\mathbf{F}_{12})_{\alpha\beta} = e^{i\left(\epsilon_\alpha - E_\beta - \frac{v_0^2}{2}\right)t}\langle\psi_\alpha(\mathbf{r}_T)|e^{i\boldsymbol{v}_0\cdot\mathbf{r}_T}(H - E_\beta)\phi_\beta(\mathbf{r}_P)\rangle, \tag{14}$$

$$(\mathbf{F}_{21})_{\beta\alpha} = e^{i(E_\beta + \frac{v_0^2}{2} - \epsilon_\alpha)t} \langle e^{i\boldsymbol{v}_0\cdot\mathbf{r}_T}\phi_\beta(\mathbf{r}_P)|(H-\epsilon_\alpha)\psi_\alpha(\mathbf{r}_T)\rangle, \tag{15}$$

$$(\mathbf{F}_{22})_{\beta\beta'} = e^{i(E_\beta - E_{\beta'})t}\langle\phi_\beta(\mathbf{r}_P)|V_P|\phi_{\beta'}(\mathbf{r}_P)\rangle, \tag{16}$$

$\alpha, \alpha'$ ($\beta, \beta'$) run from 1 to $N$ ($M$), and † indicates Hermitian conjugate. $\mathbf{F}_{11}$ and $\mathbf{F}_{22}$ represent direct interactions, and $\mathbf{F}_{12}$ and $\mathbf{F}_{21}$ describe electron transfer between the projectile and target nuclei. $\mathbf{S}$, $\mathbf{F}_{11}$, and $\mathbf{F}_{22}$ are Hermitian matrices but

$$\begin{aligned}(\mathbf{F}_{21}^\dagger)_{\alpha\beta} = (\mathbf{F}_{12})_{\alpha\beta} + e^{i\left(\epsilon_\alpha - E_\beta - \frac{v_0^2}{2}\right)t} \\ \times\left[\left(\frac{v_0^2}{2} + E_\beta - \epsilon_\alpha\right)\langle\psi_\alpha(\mathbf{r}_T)|e^{i\boldsymbol{v}_0\cdot\mathbf{r}_T}\phi_\beta(\mathbf{r}_P)\rangle\right. \\ \left. - i\boldsymbol{v}_0\cdot\langle\psi_\alpha(\mathbf{r}_T)|e^{i\boldsymbol{v}_0\cdot\mathbf{r}_T}(\boldsymbol{\nabla}_P\phi_\beta(\mathbf{r}_P))\rangle\right].\end{aligned} \tag{17}$$

The result (17) is needed to show that the normalization of the wave function $\Psi$ remains constant in time, i.e.,

$$\frac{d}{dt}\langle\Psi|\Psi\rangle = \frac{d}{dt}(\mathbf{A}^\dagger\mathbf{S}\mathbf{A}) = 0. \tag{18}$$

From (18) it follows that

$$\mathbf{A}^\dagger\mathbf{A}(t=-\infty) = \mathbf{A}^\dagger\mathbf{A}(t=+\infty) \tag{19}$$

since, from (10) and (11), $\mathbf{S}(t=-\infty) = \mathbf{S}(t=+\infty) = \mathbf{I}$. Thus, probability is conserved, as required. The evaluation of the matrix elements needed in (11), (14), and (15) is described in the Appendix.

If the electronic states $\psi_\alpha$ and $\phi_\beta$ are quantized along the direction of $\boldsymbol{v}_0$ with magnetic quantum numbers $m_\alpha$ and $m_\beta$, respectively, then, as in [21], it can be shown that dependence on the azimuthal angle $\phi_b$ of the impact parameter $\mathbf{b}$ may be removed from Eqs. (8). Specifically (see the Appendix, for example), it can be shown that

$$A_\gamma(\mathbf{b},t) = e^{-im_\gamma\phi_b}\overline{A}_\gamma(b,t), \tag{20}$$

$$S_{\gamma\delta}(\mathbf{b},t) = e^{i(m_\delta - m_\gamma)\phi_b}\overline{S}_{\gamma\delta}(b,t), \tag{21}$$

$$F_{\gamma\delta}(\mathbf{b},t) = e^{i(m_\delta - m_\gamma)\phi_b}\overline{F}_{\gamma\delta}(b,t). \tag{22}$$

If the equations are then solved subject to

$$\overline{A}_\gamma(b,-\infty) = \delta_{\gamma 0}, \tag{23}$$

it follows that the solution of Eqs. (8) with

$$A_\gamma(\mathbf{b},-\infty) = \delta_{\gamma 0} \tag{24}$$

is

$$A_\gamma(\mathbf{b},t) = e^{i(m_0 - m_\gamma)\phi_b}\overline{A}_\gamma(b,t). \tag{25}$$

Further, as in [21], it can be shown that (see the Appendix)

$$\overline{S}_{\gamma',-m_\gamma;\delta',-m_\delta} = (-1)^{m_\delta - m_\gamma}\overline{S}_{\gamma' m_\gamma;\delta' m_\delta} \tag{26}$$

and similarly $\overline{F}$, where we write $\gamma \equiv \gamma' m_\gamma$, with $\gamma'$ standing for quantum numbers other than $m_\gamma$. If $m_0 = 0$, it follows that

$$\overline{A}_{\gamma',-m_\gamma} = (-1)^{m_\gamma}\overline{A}_{\gamma' m_\gamma} \tag{27}$$

so we need only consider non-negative values of the magnetic quantum numbers in solving Eqs. (8), thereby reducing the labor by a factor of 2.

### B. Connection with wave treatment

In the wave treatment, and in the relative coordinate system ("center-of-mass coordinate system") in which the target is treated as if it were at rest, the differential cross section for scattering of the projectile is given by

$$\frac{d\sigma_{f0}}{d\Omega_P} = \mu_f^2\frac{v_f'}{v_0}|f_{f0}|^2, \tag{28}$$

where $\mu_f$ is the reduced mass in the final state. Here, for the moment, we consider only final states in which the electron is bound to the target nucleus [$(T+e)$ type, where $T$ denotes target nucleus] or bound to the projectile nucleus [$(P+e)$ type). Ionized final states are addressed in Sec. II C. The velocity $\boldsymbol{v}_f'$ is that of the center of mass (c.m.) of the scattered system [$P$ or $(P+e)$] relative to the c.m. of the final target state [$(T+e)$ or $T$]. The scattering amplitude is given by

$$\begin{aligned}f_{f0} &= -\frac{1}{2\pi}\langle e^{i\mu_f\boldsymbol{v}_f'\cdot\mathbf{R}_P}\psi_f(\mathbf{r}_T)|V_T|\Psi^+\rangle, \\ \mu_f &\equiv M_P(M_T+1)/(M_P+M_T+1),\end{aligned} \tag{29}$$

for $(T+e)$-type final states, and by

$$\begin{aligned}f_{f0} &= -\frac{1}{2\pi}\langle e^{i\mu_f\boldsymbol{v}_f'\cdot\mathbf{R}_{Pe}}\phi_f(\mathbf{r}_P)|V_P|\Psi^+\rangle, \\ \mu_f &\equiv (M_P+1)M_T/(M_P+M_T+1),\end{aligned} \tag{30}$$

for $(P+e)$ final states. In (29) and (30), $\mathbf{R}_P$ ($\mathbf{R}_{Pe}$) is the position vector of the projectile nucleus [$(P+e)$ c.m.] relative to the $(T+e)$ c.m. (target nucleus), $\psi_f$ and $\phi_f$ are the final states of the electron, and $\Psi^+$ is the full scattering wave function of the system with outgoing scattered waves:

$$\begin{aligned}\Psi^+ &\xrightarrow{\text{asymp.}} e^{i\mu_i\boldsymbol{v}_0\cdot\mathbf{R}_P}\psi_0(\mathbf{r}_T) + \text{outgoing scattered waves}, \\ \mu_i &\equiv M_P(M_T+1)/(M_P+M_T+1),\end{aligned} \tag{31}$$

with $\psi_0$ being the initial state of the target electron.

To make the connection with the impact parameter approximation we follow the line of argument of [21]. In [21] there were only $(T+e)$-type channels. The difference here is the presence of charge exchange $(P+e)$ final states. So let us concentrate upon these. In the first Born approximation the amplitude for a transition to a final $(P+e)$-type channel is [see Eqs. (2), (5), (30), and (31)]

$$\begin{aligned}f_{f0}^{B1} = -\frac{1}{2\pi}\int e^{-i\mu_f\boldsymbol{v}_f'\cdot\mathbf{R}_{Pe}}\phi_f^*(\mathbf{r}_P) \\ \times\left(\frac{Z_P Z_T}{R} - \frac{Z_T}{r_T}\right)e^{i\mu_i\boldsymbol{v}_0\cdot\mathbf{R}_P}\psi_0(\mathbf{r}_T)d\mathbf{R}_P d\mathbf{r}_T\end{aligned} \tag{32}$$

where * denotes complex conjugation. After some manipulation (32) can be written (exactly) as [35]

$$\begin{aligned}f_{f0}^{B1} &= -\frac{1}{2\pi}\int e^{i\mathbf{q}\cdot\mathbf{R}}e^{-i\boldsymbol{v}_f\cdot\mathbf{r}_T}\phi_f^*(\mathbf{r}_T-\mathbf{R}) \\ &\quad\times\left(\frac{Z_P Z_T}{R} - \frac{Z_T}{r_T}\right)\psi_0(\mathbf{r}_T)d\mathbf{R}_P d\mathbf{r}_T, \\ &= -\frac{1}{2\pi}\int e^{i\mathbf{q}\cdot\mathbf{R}}\langle e^{i\boldsymbol{v}_f\cdot\mathbf{r}_T}\phi_f(\mathbf{r}_P)|V_P|\psi_0(\mathbf{r}_T)\rangle d\mathbf{R},\end{aligned} \tag{33}$$

where $\boldsymbol{v}_f$ is the final velocity of the c.m. of the $(P+e)$ system in the laboratory and

$$\mathbf{q} \equiv M_P(\boldsymbol{v}_0 - \boldsymbol{v}_f). \tag{34}$$

Making the approximation outlined in [21], i.e.,

$$\boldsymbol{v}_f \approx \boldsymbol{v}_0 + O(1/M), \tag{35}$$

where $M$ is a typical nuclear mass (an excellent approximation at all but the lowest impact energies), (33) may be written

$$f_{f0}^{B1} = -\frac{1}{2\pi}\int\left[\int_{-\infty}^{\infty} e^{i\left(E_f+\frac{v_0^2}{2}-\epsilon_0\right)t} \times \langle e^{i\boldsymbol{v}_0\cdot\mathbf{r}_T}\phi_f(\mathbf{r}_P)|V_P|\psi_0(\mathbf{r}_T)\rangle dt\right] e^{i\mathbf{q}\cdot\mathbf{b}}d^2\mathbf{b}. \tag{36}$$

This is now recognized as

$$f_{f0}^{B1} = -\frac{v_0 i}{2\pi}\int e^{i\mathbf{q}\cdot\mathbf{b}} b_f^{B1}(\mathbf{b},\infty)d^2\mathbf{b}, \tag{37}$$

where $b_f^{B1}$ is the corresponding first Born approximation to the coupled Eqs. (8) obtained on taking

$$a_\alpha(\mathbf{b},-\infty) = \delta_{\alpha 0}, \quad b_\beta(\mathbf{b},-\infty) = 0 \tag{38}$$

[see Eqs. (5), (8), (9), and (15)]. This is exactly the same form of result as is obtained for the $(T+e)$ channels; see [21]. Thus, in general [36],

$$f_{f0}^{B1} = -\frac{v_0 i}{2\pi}\int e^{i\mathbf{q}\cdot\mathbf{b}}\left[A_f^{B1}(\mathbf{b},\infty) - \delta_{f0}\right]d^2\mathbf{b} \tag{39}$$

for any final channel $f$.

By considering an iterative solution, as in [21], of Eqs. (8) and the corresponding wave version [37] we conclude that for the full scattering amplitude, in the approximation (35),

$$\begin{aligned} f_{f0} &= -\frac{v_0 i}{2\pi}\int e^{i\mathbf{q}\cdot\mathbf{b}}[A_f(\mathbf{b},\infty) - \delta_{f0}]d^2\mathbf{b}, \\ &= -v_0 i^{m_f-m_0+1}e^{i(m_0-m_f)\phi_q} \\ &\quad\times\int_0^\infty J_{(m_f-m_0)}(q_t b)(\overline{A}_f(b,\infty) - \delta_{f0})bdb \end{aligned} \tag{40}$$

(see [21]), where $J_M$ is a Bessel function and $q_t$ is the magnitude of the transverse component of $\mathbf{q}$, i.e., perpendicular to $\boldsymbol{v}_0$.

### C. Ionization

The total ionization cross section is calculated from

$$\sigma_{\rm ion} = \sum_{\alpha=1}^{N}\sigma_\alpha^D g_\alpha + \sum_{\beta=1}^{M}\sigma_\beta^E h_\beta, \tag{41}$$

where

$$\begin{aligned} \sigma_\alpha^D &= \int |a_\alpha(\mathbf{b},\infty)|^2 d^2\mathbf{b}, \\ \sigma_\beta^E &= \int |b_\beta(\mathbf{b},\infty)|^2 d^2\mathbf{b}, \end{aligned} \tag{42}$$

and $g_\alpha$ ($h_\beta$) is the fraction of the target state $\psi_\alpha$ (projectile state $\phi_\beta$) lying in the continuum [21]. The sum over the target states ($\alpha$) in (41) corresponds to direct ionization, and that over the projectile states ($\beta$) represents charge exchange to the continuum of the projectile [29,30].

Our interest here, however, is primarily differential ionization. For this we first turn to the wave expression for the ionization amplitude,

$$f_{\rm ion} = -\frac{1}{2\pi}\langle\Psi_f|V_I|\Psi^+\rangle, \tag{43}$$

where $\Psi_f$ represents the final state of the projectile and ionized electron and $H = H_I + V_I$. By an appropriate choice of $H_I$ we can take into account explicitly whatever interactions we consider to be important in the final state. The choice of $H_I$ matters not if $\Psi^+$ is exact, but if $\Psi^+$ is approximated it does matter [38]. Let the ionized electron be moving with velocity (momentum) $\boldsymbol{\kappa}$ in the laboratory (where the target is initially at rest). If its velocity is low relative to the target nucleus then an appropriate choice for $H_I$ is $H_T$, as in [21]. This leads to the amplitude expression [see (29)]

$$f_{\rm ion} = -\frac{1}{2\pi}\left\langle e^{i\mu_f\boldsymbol{v}_f'\cdot\mathbf{R}_P}\psi_{\boldsymbol{\kappa}}^-(\mathbf{r}_T)|V_T|\Psi^+\right\rangle. \tag{44}$$

However, if the electron is moving with the projectile (charge exchange to the continuum), a better choice would be $H_I = H_P$, leading to [see (30)]

$$f_{\rm ion} = -\frac{1}{2\pi}\left\langle e^{i\mu_f\boldsymbol{v}_f'\cdot\mathbf{R}_P e}\phi_{(\boldsymbol{\kappa}-\boldsymbol{v}_P)}^-(\mathbf{r}_P)|V_P|\Psi^+\right\rangle, \tag{45}$$

where $\phi_{\boldsymbol{\kappa}'}^-$ is the wave function for an electron of momentum $\boldsymbol{\kappa}'$ relative to the projectile nucleus and $\boldsymbol{v}_P$ is the final velocity of the projectile nucleus in the laboratory.

To extract the differential motion of the electron from the pseudostates we assume that they are, for matrix element purposes, a good approximation to a complete set. Thus, if the states $\psi_\alpha(\mathbf{r}_T)$ are such, then inserting them into (44) we get, as in [21],

$$\begin{aligned} &-\frac{1}{2\pi}\sum_{\alpha=1}^{N}\langle\psi_{\boldsymbol{\kappa}}^-(\mathbf{r}_T)|\psi_\alpha(\mathbf{r}_T)\rangle\left\langle e^{i\mu_f\boldsymbol{v}_f'\cdot\mathbf{R}_P}\psi_\alpha(\mathbf{r}_T)|V_T|\Psi^+\right\rangle \\ &\equiv f_{\rm ion}^T \quad \text{(say)}. \end{aligned} \tag{46}$$

Similarly, if the states $\phi_\beta(\mathbf{r}_P)$ were effectively complete, (45) could be written

$$\begin{aligned} &-\frac{1}{2\pi}\sum_{\beta=1}^{M}\langle\phi_{(\boldsymbol{\kappa}-\boldsymbol{v}_P)}^-(\mathbf{r}_P)|\phi_\beta(\mathbf{r}_P)\rangle\left\langle e^{i\mu_f\boldsymbol{v}_f'\cdot\mathbf{R}_{Pe}}\phi_\beta(\mathbf{r}_P)|V_P|\Psi^+\right\rangle \\ &\equiv f_{\rm ion}^P \quad \text{(say)}. \end{aligned} \tag{47}$$

But, if $\Psi^+$ is approximated as in [37] then for $R$ greater than some $R_0$ the overlap between the states $\psi_\alpha(\mathbf{r}_T)$ and $\phi_\beta(\mathbf{r}_P)$ becomes negligible and so (46) does not pick up that part of the wave function $\Psi^+$ coming from the $\phi_\beta$ components, i.e., the charge exchange to the continuum channels. This probably would not matter much if $\boldsymbol{\kappa}$ were small and the final state interaction between the ionized electron and the target nucleus were dominant. But it might make a lot of difference if the electron were ejected into a low-velocity state relative to the projectile nucleus, i.e., $(\boldsymbol{\kappa} - \boldsymbol{v}_P)$ small. The situation for the approximation (47) is the opposite way around: one might expect it to do well for low $(\boldsymbol{\kappa} - \boldsymbol{v}_P)$ but to be poor for low $\boldsymbol{\kappa}$. It

seems that both situations might be covered by simply adding (46) and (47), i.e., by forming the "coherent" combination

$$f_{\rm ion}^{\rm CO} = f_{\rm ion}^{T} + f_{\rm ion}^{P} \tag{48}$$

with the triple differential cross section (TDCS) therefore being proportional to [see (55)]

$$\left| f_{\rm ion}^{T} + f_{\rm ion}^{P} \right|^2. \tag{49}$$

However, for $R < R_0$ there is overlap between the states $\psi_\alpha(\mathbf{r}_T)$ and $\phi_\beta(\mathbf{r}_P)$ and so we are double counting in some way.

A different viewpoint comes from the total cross section ansatz (41), where the cross section is obtained from an "incoherent" combination of the amplitudes $a_\alpha$ and $b_\beta$. This formulation is consistent with the unitarity (19) of the approximation. This suggests we should take the incoherent combination

$$\text{TDCS} \propto \left| f_{\rm ion}^{T} \right|^2 + \left| f_{\rm ion}^{P} \right|^2. \tag{50}$$

We explore both possibilities (49) and (50).

Finally, we use (40) to write [39]

$$f_{\rm ion}^{T} = -i v_0 \sum_{\alpha=1}^{N} \langle \psi_{\boldsymbol{\kappa}}^{-}(\mathbf{r}_T) | \psi_\alpha(\mathbf{r}_T) \rangle i^{m_\alpha - m_0} e^{i(m_0 - m_\alpha)\phi_q} \times \int_0^\infty J_{(m_\alpha - m_0)}(q_t b)(\overline{a}_\alpha(b,\infty) - \delta_{\alpha 0}) b db, \tag{51}$$

$$f_{\rm ion}^{P} = -i v_0 \sum_{\beta=1}^{M} \left\langle \phi_{(\boldsymbol{\kappa} - \boldsymbol{v}_P)}^{-}(\mathbf{r}_P) | \phi_\beta(\mathbf{r}_P) \right\rangle i^{m_\beta - m_0} e^{i(m_0 - m_\beta)\phi_{q'}} \times \int_0^\infty J_{(m_\beta - m_0)}(q_t' b) \overline{b}_\beta(b,\infty) b db, \tag{52}$$

where now

$$\mathbf{q} \equiv M_P(\boldsymbol{v}_0 - \boldsymbol{v}_P) \tag{53}$$

is the momentum transfer to the projectile and

$$\mathbf{q}' \equiv \mathbf{q} - \boldsymbol{\kappa} \tag{54}$$

is the momentum transfer to the "projectile + electron." Note that in obtaining (52) from (40) we must take $\boldsymbol{v}_f$ in (34) to be the velocity of the center of mass of the $(P + e)$ system, which for ionization is $(M_P \boldsymbol{v}_P + \boldsymbol{\kappa})/(M_P + 1)$. Then, recognizing that $\boldsymbol{v}_P = \boldsymbol{v}_0 + O(1/M_P)$ and that $\boldsymbol{v}_0 \cdot \mathbf{b} = 0$, and dropping terms of order $1/M_P$, $\mathbf{q} \cdot \mathbf{b}$ in (40) becomes $\mathbf{q}' \cdot \mathbf{b}$, and (52) follows.

## III. RESULTS

We present results for proton impact on atomic hydrogen at an impact energy of 75 keV where there are interesting double differential measurements [18,19]. We show calculations of the TDCS as observed in the laboratory [21], i.e.,

$$\frac{d^3\sigma^L}{dE d\Omega_e d\Omega_P} = \frac{v_f \kappa}{v_0} M_P^2 |f_{\rm ion}|^2. \tag{55}$$

This is the cross section for the electron being ejected with energy in the range $E$ to $E + dE$ and into the solid angle $d\Omega_e$ while the projectile is scattered into the solid angle $d\Omega_P$. In (55), $\boldsymbol{v}_0$, $\boldsymbol{v}_f$, and $\boldsymbol{\kappa}$ are respectively the incident and final velocity of the projectile, and the momentum of the ejected electron, all as observed in the laboratory. We study the different options (49) ("coherent") and (50) ("incoherent") for determining the TDCS and show how the individual contributions of $|f_{\rm ion}^{T}|^2$ and $|f_{\rm ion}^{P}|^2$ compare.

We begin by looking at integrated cross sections which we can compare with the extensive work of Winter [34], who, as here, has also used pseudostates (he calls them "Sturmians") in the time-dependent impact parameter approximation. His largest calculation employs $s$, $p$, $d$, and $f$ states up to $n = 13$ [40] on both the projectile and the target. We use the same number but with a different pseudostate basis. Taking advantage of the symmetry (27) this results in 220 complex coupled equations, or equivalently 440 real equations. While the two pseudostate bases are not the same we would expect to get comparable results if there is convergence.

For our basis we have taken the Laguerre functions [21,41]

$$\chi_{klm}(\mathbf{r}) = (\lambda_l r)^l L_{k-1}^{2l+2}(\lambda_l r) e^{-\lambda_l r/2} Y_{lm}(\hat{\mathbf{r}}), \quad k = 1, \ldots, 15 - l, \quad l = 0, \ldots, 3, \tag{56}$$

with $\lambda_l = 2.1559$, $2.2453$, $2.4068$, $2.6391$ for $l = 0, \ldots, 3$ respectively. Diagonalizing $H_T$ (equivalently $H_P$), this generates states up to $n = 15$. We remove the high-energy $n = 14$ and 15 states to help ease problems with linear dependence. The choice of the values of $\lambda_l$ ensures that the $n = 7$ states have an energy of 5 eV, which means that for a 5-eV ejected electron $f_{\rm ion}^{T}$ is calculated in the unrelaxed approximation of [21] rather than the relaxed approximation of [25]. This is an arbitrary question of taste. The $n = 1$ and 2 states obtained from the diagonalization are excellent approximations to the corresponding eigenstates; the $n = 3$ states are good approximations. The integrated discrete direct and exchange cross sections are calculated from

$$\int |a_\alpha(\mathbf{b},\infty) - \delta_{\alpha 0}|^2 d^2\mathbf{b}, \qquad \int |b_\beta(\mathbf{b},\infty)|^2 d^2\mathbf{b}, \tag{57}$$

respectively, and the integrated ionization cross section from (41). Finally, we integrate the coupled Eqs. (8) over $z = v_0 t$ from $z = -10^6$ a.u. to $+10^6$ a.u. but only switch on the exchange interaction ($\mathbf{F}_{12}$ and $\mathbf{F}_{21}$) between $z = -35$ a.u. to $+35$ a.u.

### A. Integrated cross sections

The results for our integrated cross sections are shown in Table I, where they are seen to be in very good agreement with the corresponding $n \leqslant 13(s,p,d,f)$ calculations of Winter [34]. About one-third of the total ionization cross section at this energy comes from charge exchange to the continuum, i.e., the second sum in (41).

### B. Triple differential cross section (TDCS)

We have calculated the TDCSs, see (55),

$$\begin{aligned} T &\equiv K \left| f_{\rm ion}^{T} \right|^2, \\ P &\equiv K \left| f_{\rm ion}^{P} \right|^2, \\ \text{INCO} &\equiv K \left( \left| f_{\rm ion}^{T} \right|^2 + \left| f_{\rm ion}^{P} \right|^2 \right), \\ \text{CO} &\equiv K \left| f_{\rm ion}^{T} + f_{\rm ion}^{P} \right|^2, \\ K &\equiv \frac{v_f \kappa}{v_0} M_P^2, \end{aligned} \tag{58}$$

TABLE I. Cross sections (in units of $10^{-17}$ cm$^2$) for proton impact on atomic hydrogen at 75 keV. Comparison is made between present results and those of Winter [34] in his $\leqslant 13(s,p,d,f)$ approximation.

(a) Direct Transitions and Ionization

| | $1s$ | $2s$ | $2p$ | $3s$ | $3p$ | $3d$ | Ionization |
|---|---|---|---|---|---|---|---|
| Present | 5.49 | 1.30 | 7.84 | 0.29 | 1.27 | 0.24 | 15.99 |
| Winter | | 1.3 | 7.5 | 0.3 | 1.2 | 0.2 | 16.1 |

(b) Exchange Transitions

| | $1s$ | $2s$ | $2p$ | $3s$ | $3p$ | $3d$ |
|---|---|---|---|---|---|---|
| Present | 2.07 | 0.45 | 0.096 | 0.149 | 0.034 | 0.0022 |
| Winter | 2.10 | 0.44 | 0.09 | 0.15 | 0.03 | 0.002 |

for ejected electron energies of 5, 10, 16.395, 26.395, and 36.395 eV and momentum transfers up to $q = 1.5$ a.u. The last three energies are those of the double differential measurements of [18,19] and correspond to energy losses of 30, 40, and 50 eV, respectively. We note that an ejected electron would need an energy of 40.85 eV in order to move at the same speed as the projectile. INCO and CO are the incoherent and coherent approximations discussed in Sec. II C; see (49) and (50). $T$ and $P$ give us some feeling for the relative importance of direct and exchange ionization. In Figs. 1–5 we show a selection of our results for coplanar geometry. We adopt the following conventions. We take the $Z$ direction to be the direction of the incident proton. The incident and scattered protons define the $X$-$Z$ plane with the scattered proton emerging on the negative $X$ side. The lowest momentum transfer $q$ in each figure corresponds to forward scattering of the proton.

Figure 1 shows the TDCS for the case of 5-eV ejection. At such a low ejection energy we would expect the electron to be largely under the influence of the target nucleus. That expectation is borne out for all our values of $q$ by the relative size of $T$ and $P$ and the consequent proximity of $T$ to INCO. However, CO indicates a larger role for $f_{\rm ion}^{P}$ with increasing $q$ [42]. $T$, INCO, and CO display clear binary and recoil peaks, although the recoil peak is very much smaller than the binary. Furthermore, both peaks are rotated away from the momentum transfer direction **q** towards the direction of the outgoing proton as the proton attracts the ejected electron towards it. This is classic behavior that has been seen in electron impact ionization [32,33,38], although in this case the peaks are repelled away from the negatively charged projectile. The reader should also be aware of the rapidly reducing size of the cross section with increasing $q$; often the most interesting features occur where the cross section is relatively small and therefore harder to measure.

Figure 2 shows the situation at 10-eV ejection energy where $T$ and $P$ are comparable at small $q$. However, with increasing $q$, $T$ begins to dominate once again. Both $T$ and $P$ show rotation away from the direction of **q** towards the outgoing proton, $P$ more so than $T$, and $T$ less so than at 5 eV; see Fig. 1. INCO also shows clear rotation and so does CO, at least up to $q = 0.77$ a.u. At $q = 0.97$ a.u. and beyond, CO is not so much rotated as structured. CO starts off being much larger than INCO, eventually becoming smaller by $q = 1.5$ a.u.

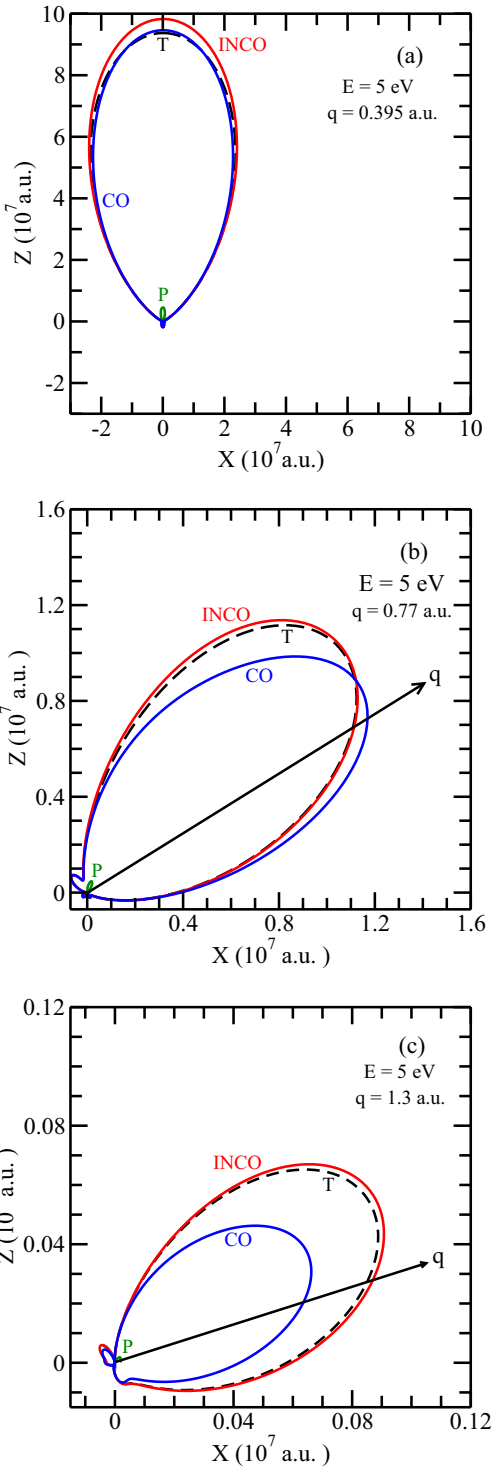


FIG. 1. (Color online) Laboratory frame TDCS (in a.u.) for proton impact ionization of atomic hydrogen at 75 keV in coplanar geometry and for an ejected electron energy, $E$, of 5 eV. (a) Forward scattering of the proton. The direction of the momentum transfer **q**, see (53), is indicated in (b) and (c). The approximations are as described in (58).

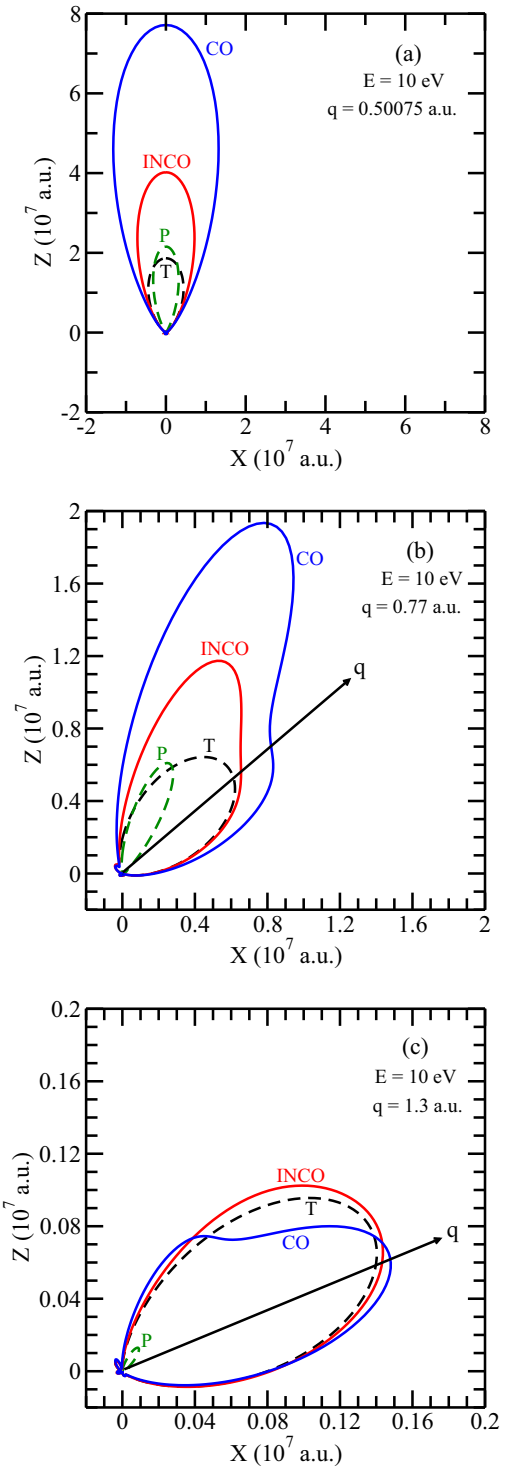


FIG. 2. (Color online) Laboratory frame TDCS (in a.u.) for proton impact ionization of atomic hydrogen at 75 keV in coplanar geometry and for an ejected electron energy, $E$, of 10 eV. (a) Forward scattering of the proton. The direction of the momentum transfer **q**, see (53), is indicated in (b) and (c). The approximations are as described in (58).

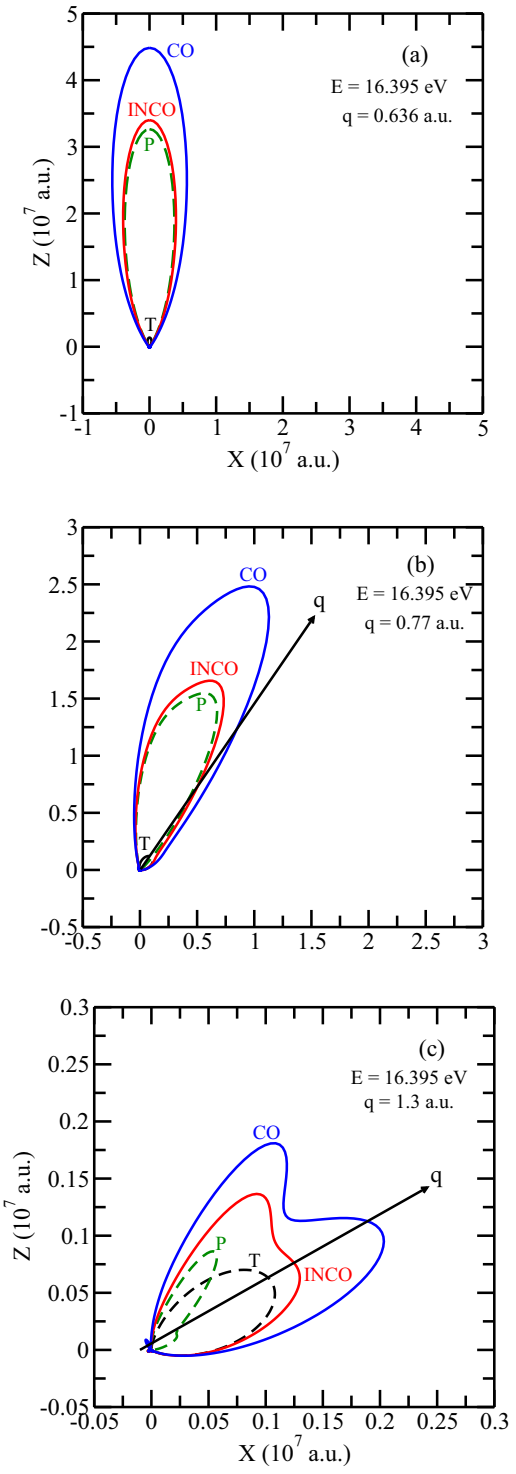


FIG. 3. (Color online) Laboratory frame TDCS (in a.u.) for proton impact ionization of atomic hydrogen at 75 keV in coplanar geometry and for an ejected electron energy, $E$, of 16.395 eV. (a) Forward scattering of the proton. The direction of the momentum transfer **q**, see (53), is indicated in (b) and (c). The approximations are as described in (58).

The results for ejection energies of 16.395 and 26.395 eV, Figs. 3 and 4, are similar in pattern to Fig. 2 except that now $P$ is very much dominant for most of the momentum range shown and for 26.395 eV ejection remains dominant up to $q = 1.5$ a.u., although $T$ is growing.

At an ejection energy of 36.395 eV, Fig. 5, the electron is now moving with a speed comparable to that of the proton

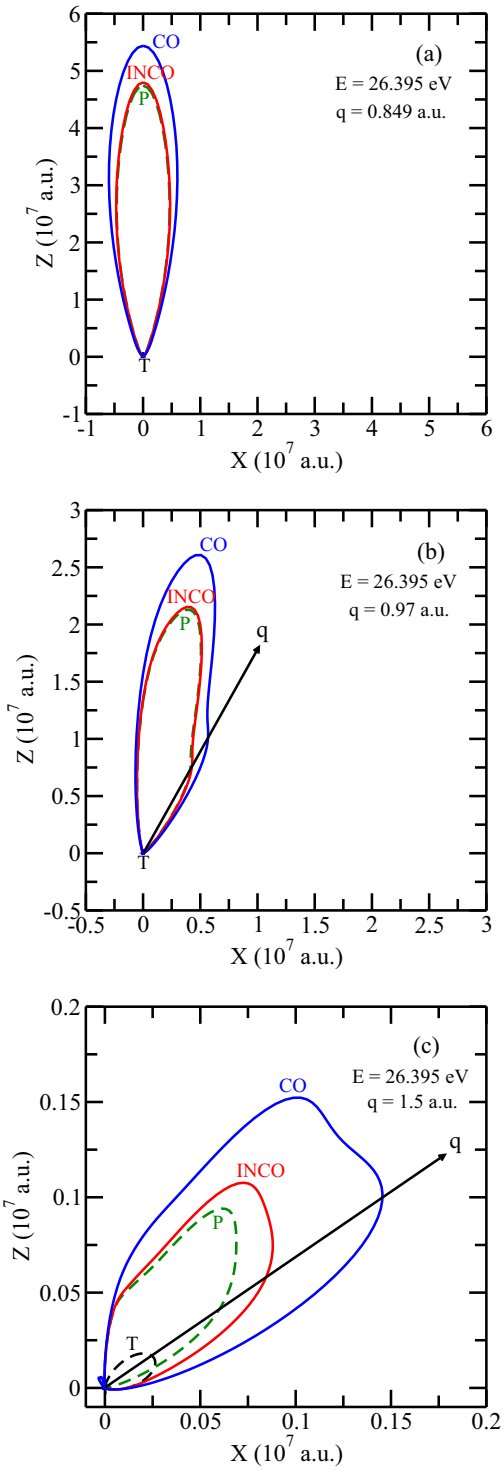


FIG. 4. (Color online) Laboratory frame TDCS (in a.u.) for proton impact ionization of atomic hydrogen at 75 keV in coplanar geometry and for an ejected electron energy, $E$, of 26.395 eV. (a) Forward scattering of the proton. The direction of the momentum transfer **q**, see (53), is indicated in (b) and (c). The approximations are as described in (58).

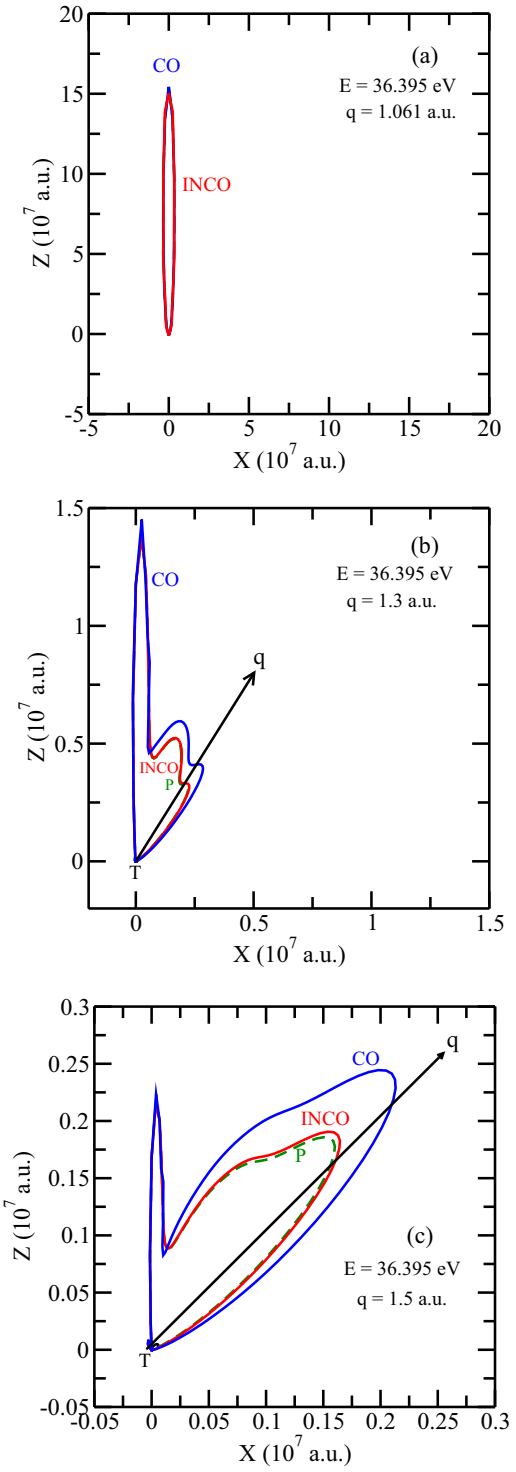


FIG. 5. (Color online) Laboratory frame TDCS (in a.u.) for proton impact ionization of atomic hydrogen at 75 keV in coplanar geometry and for an ejected electron energy, $E$, of 36.395 eV. (a) Forward scattering of the proton. The direction of the momentum transfer **q**, see (53), is indicated in (b) and (c). The approximations are as described in (58).

and so we would expect to see $P$ very dominant, and indeed we do. For forward scattering, Fig. 5(a), the electron is very much dragged behind the proton, resulting in a cross section that looks like a spike. This forward spike also persists at $q = 1.3$ a.u. and 1.5 a.u. [Figs. 5(b) and 5(c)], although now a smoother structure develops (both in INCO and CO) towards the direction of **q** but rotated from it towards the outgoing proton.

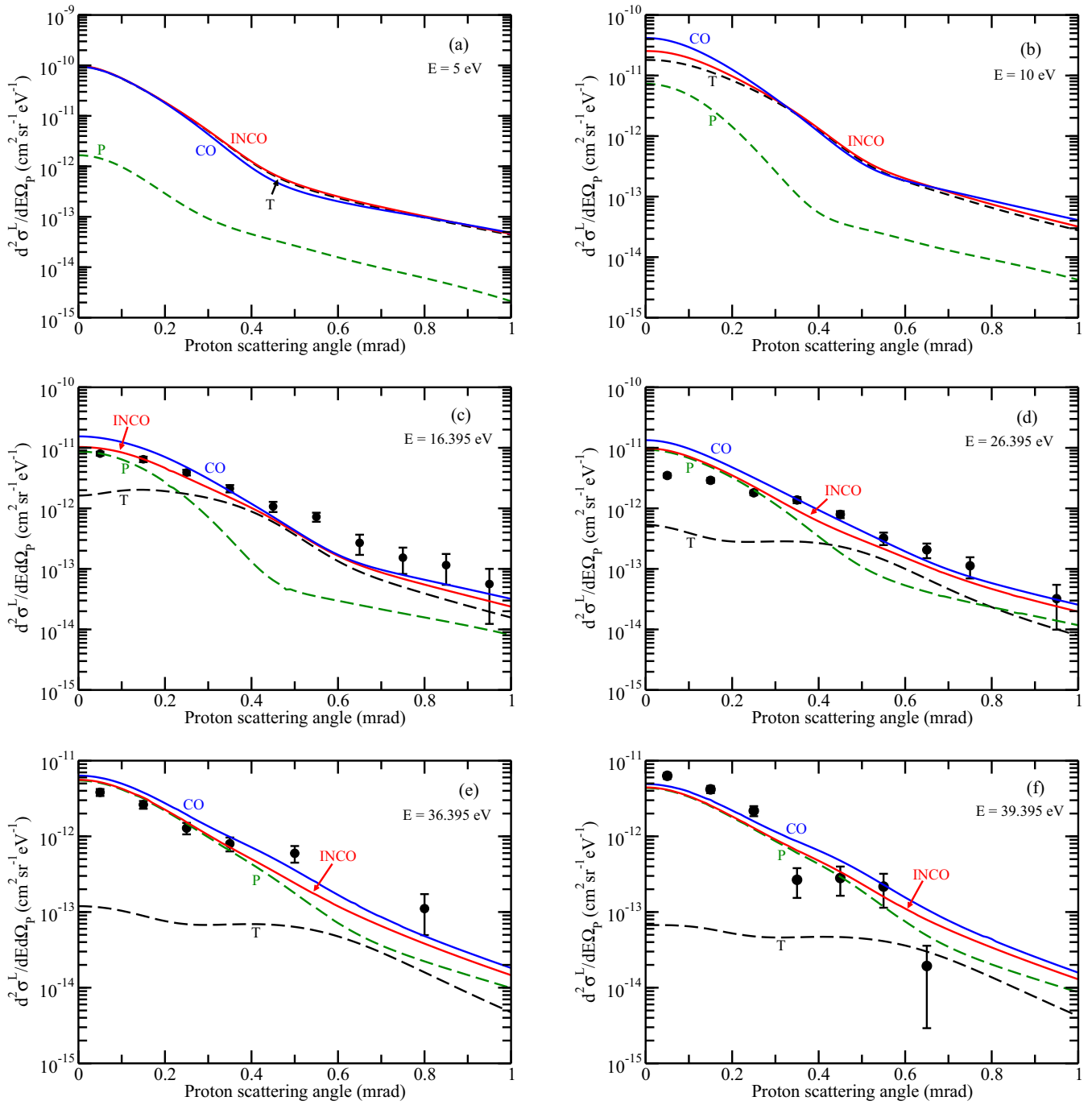


FIG. 6. (Color online) Laboratory frame double differential cross section (59) for proton impact ionization of atomic hydrogen at 75 keV and for ejected electron energies $E$ as indicated. The approximations are as described in (58). INCO, red solid curve; CO, blue solid curve; $T$, black dashed curve; $P$, green dashed curve. The experimental data are from [18,19].

### C. Double differential cross section $d^2\sigma^L/dEd\Omega_p$

In Fig. 6 we show the double differential cross section (DDCS)

$$\frac{d^2\sigma^L}{dEd\Omega_P} = \int \frac{d^3\sigma^L}{dEd\Omega_e d\Omega_P} d\Omega_e, \tag{59}$$

as observed in the laboratory for electron ejection energies of 5, 10, 16.395, 26.395, 36.395, and 39.395 eV. As for the TDCS we plot the contributions $T$, $P$, INCO and CO; see (58). We also make comparison with the absolute experimental data from [18,19]. Figure 6(a) shows the case of 5-eV electron ejection and, as expected from Fig. 1, we see that $T$ dominates $P$ at all of the angles shown [43]. The result is that INCO lies close to $T$ and that there is little difference between INCO and CO.

Figure 6(b) corresponds to 10-eV ejection energy. Again $T$ dominates $P$ at all angles but $P$ approaches $T$ towards the forward direction. Again this is consistent with Fig. 2, where we saw that $P$ rapidly becomes smaller than $T$ with increasing

momentum transfer $q$ and that, although comparable to $T$ at small $q$, the narrowness of the binary peak as compared to that of $T$ should integrate out to give a smaller DDCS. Except near the forward direction, INCO and CO remain close. In the forward region CO is larger than INCO, as we might expect from Fig. 2.

At 16.395 eV, Fig. 6(c), $P$ now dominates $T$ near the forward direction but, consistent with Fig. 3, becomes smaller than $T$ beyond 0.24 mrad [43]. In this case we now have experimental data from [18,19]. The measurements tend to prefer INCO at small angles although there is not that much difference between CO and INCO. At the larger angles experiment tends to lie above both INCO and CO.

As the ejection energy is increased to 26.395 eV, Fig. 6(d), $P$ becomes ever more dominant over $T$ in the forward region and even exceeds $T$ at the largest angles shown [43]. Note that both INCO and CO lie above the experimental data in the forward angular region while the measurements are generally in agreement with CO, but not INCO, at large angles.

At the ejection energies of 36.395 and 39.395 eV, Figs. 6(e) and 6(f), unsurprisingly (see Figs. 4 and 5), $P$ dominates $T$ at all the angles shown. In the forward angular region the experimental data lie below both INCO and CO at 36.395 eV and above at 39.395 eV; at larger angles the reverse tends to be true.

It is clear from Fig. 6 that the experimental data do not show a systematic behavior relative to INCO or CO and, even if they did, the error bars would probably be too large to discriminate between INCO and CO. Schulz *et al.* [18,19] describe carefully how their measured DDCS is normalized. They remark that, because of uncertainty in the normalization procedure, differences in overall normalization between theory and experiment are not necessarily significant. However, it is clear from Fig. 6 that renormalization of the experimental data to either the INCO or CO curves would still not bring overall agreement with experiment. Since the publication of [18,19] it has emerged that there can be problems with the coherence of ion beams [44–46]. This depends on the width of the collimating slit and the distance of the source from the target region. To what extent the measurements of [18,19] may be affected by this has not been made clear. A further experimental check would be in order.

It is interesting to integrate the DDCS (59) over the ejected energy, $dE$, and the scattering solid angle $d\Omega_P$ to get the integrated ionization cross section at 75 keV. This is not guaranteed to be equal to the integrated ionization cross section as calculated from (41) (see Table I), but for INCO should be very close; see [25]. Our results are shown in Table II where they are also compared with the experimental measurement from [47]. It is seen that INCO gives good agreement, within numerical rounding error, with our result from Table I but CO gives a value some 14% higher. While INCO is in disagreement with experiment at this energy, being too large, as is the work of Winter [34] over a wider energy range around 75 keV, CO increases this discrepancy. That is not to say that experiment is correct.

TABLE II. Ionization cross section (in units of $10^{-17}$ cm$^2$) for proton impact on atomic hydrogen at 75 keV.

| From Table I | | | | |
|---|---|---|---|---|
| CO | INCO | Present | Winter | Experiment [47] |
| 18.3 | 16.2 | 15.99 | 16.1 | $12.91 \pm 0.41$ |

## IV. CONCLUSIONS

We have developed an approximation for differential ionization within a two-center pseudostate formalism. The approximation is fully quantal and includes the interaction between the projectile and target nuclei (the "PT" interaction of [19]) as well as post-collisional interactions between the ionized electron and the nuclei. We have shown calculations of the triple (fully) differential cross section for proton impact ionization of atomic hydrogen at 75 keV. These calculations illustrate how the post-collisional interaction switches from the situation where it is dominated by that between the electron and the target nucleus to one where the ionized electron interacts most strongly with the projectile nucleus: the so-called charge exchange to the continuum [29,30]. The extraction of the differential ionization follows the plan outlined for the earlier one-center pseudostate approximation of [21]. Whereas this plan was unambiguous for the one-center approximation, for two centers an ambiguity arises. Two options for dealing with the ambiguity have been considered, the first described as a "coherent" approach, the second as "incoherent." We have illustrated the differences between these two approaches. The most attractive feature of the incoherent approximation is that it is consistent with the basic unitarity of the approximation; it is our prejudice that this is the way to go. One might ask if there is a better approach. In principle, yes, but that would require a choice of $H_I$ in (43) in which the electron interacts with both nuclei simultaneously (i.e., solving an electron-molecule scattering problem at all distances between the nuclei) and would lead to a very complicated computational scheme. It is best, first, to try the present approach.

What therefore is needed is a good experimental test. Unfortunately, for proton impact ionization of atomic hydrogen fully differential measurements are not available, but there are double differential measurements from [18,19]. We have made comparison with these data and, while the overall comparison is encouraging, detailed agreement is lacking. However, the aforementioned measurements were made before the discovery of coherence problems with ion beams [44–46]. It is therefore essential that their sensitivity to beam coherence be investigated.

## ACKNOWLEDGMENTS

We are indebted to Prof. M. Schulz for providing us with a tabulation of the double differential measurements.

## APPENDIX

Here we show how the matrix elements required in (11), (14), and (15) are evaluated. In these cases we also make explicit the relations (21), (22), and (26) for $\mathbf{S}_{12}$, $\mathbf{F}_{12}$, and $\mathbf{F}_{21}$.

With quantization axis along the direction of $\boldsymbol{v}_0$ we separate $\psi_\alpha(\mathbf{r}_T)$ and $\phi_\beta(\mathbf{r}_P)$ into radial and angular components according to

$$\psi_\alpha(\mathbf{r}_T) = R_{n_\alpha l_\alpha}(r_T) Y_{l_\alpha m_\alpha}(\hat{\mathbf{r}}_T), \tag{A1}$$

$$\phi_\beta(\mathbf{r}_P) = S_{n_\beta l_\beta}(r_P) Y_{l_\beta m_\beta}(\hat{\mathbf{r}}_P), \tag{A2}$$

where $\hat{}$ denotes a unit vector and $Y_{lm}$ is a spherical harmonic as defined by Rose [48]. We also need

$$e^{i\boldsymbol{v}_0\cdot\mathbf{r}_T} = \sum_{l=0}^{\infty} \sqrt{4\pi(2l+1)}\, i^l\, j_l(v_0 r_T) Y_{l0}(\hat{\mathbf{r}}_T) \tag{A3}$$

and the result [49] (note that $\mathbf{r}_P = \mathbf{r}_T - \mathbf{R}$)

$$|\mathbf{r}_T - \mathbf{R}|^{l_\beta} Y_{l_\beta m_\beta}(\widehat{\mathbf{r}_T - \mathbf{R}}) = \sum_{l=0}^{l_\beta} \sum_{m=-l}^{l} (-1)^{l+l_\beta} f(l_\beta,l) C(l,l_\beta - l,l_\beta; m,m_\beta - m,m_\beta) r_T^l R^{l_\beta - l} Y_{lm}(\hat{\mathbf{r}}_T) Y_{(l_\beta - l),(m_\beta - m)}(\hat{\mathbf{R}}), \tag{A4}$$

where

$$f(l_\beta,l) \equiv \left[\frac{4\pi(2l_\beta+1)!}{(2l+1)!(2l_\beta - 2l + 1)!}\right]^{1/2} \tag{A5}$$

and $C(l_1,l_2,l_3;m_1,m_2,m_3)$ is a Clebsch-Gordan coefficient as defined by Rose [48]. Also, defining

$$S^\lambda_{n_\beta l_\beta}(r_T,R) \equiv \int_{-1}^{+1} d(\cos\theta) P_\lambda(\cos\theta) \frac{S_{n_\beta l_\beta}(|\mathbf{r}_T - \mathbf{R}|)}{|\mathbf{r}_T - \mathbf{R}|^{l_\beta}}, \tag{A6}$$

where

$$\theta = \cos^{-1}(\hat{\mathbf{r}}_T \cdot \hat{\mathbf{R}}), \tag{A7}$$

we can write

$$\frac{S_{n_\beta l_\beta}(r_P)}{r_P^{l_\beta}} = 2\pi \sum_{\lambda=0}^{\infty} \sum_{\mu=-\lambda}^{+\lambda} S^\lambda_{n_\beta l_\beta}(r_T,R) Y_{\lambda\mu}(\hat{\mathbf{r}}_T) Y^*_{\lambda\mu}(\hat{\mathbf{R}}). \tag{A8}$$

Now all the elements of

$$\left\langle \psi_\alpha(\mathbf{r}_T) | \phi_\beta(\mathbf{r}_P) e^{i\boldsymbol{v}_0\cdot\mathbf{r}_T} \right\rangle \tag{A9}$$

may be expressed in terms of $r_T$, $R$ and spherical harmonics in $\hat{\mathbf{r}}_T$, and $\hat{\mathbf{R}}$. By applying the result [48]

$$Y_{l_1 m_1}(\hat{\mathbf{r}}) Y_{l_2 m_2}(\hat{\mathbf{r}}) = \sum_{l_3=|l_1-l_2|}^{|l_1+l_2|} g(l_1,l_2;l_3) C(l_1,l_2,l_3;0,0,0) C((l_1,l_2,l_3;m_1,m_2,m_3) Y_{l_3 m_3}(\hat{\mathbf{r}}), \tag{A10}$$

where

$$g(l_1,l_2;l_3) \equiv \left[\frac{(2l_1+1)(2l_2+1)}{4\pi(2l_3+1)}\right]^{1/2}, \tag{A11}$$

the product of spherical harmonics in $\hat{\mathbf{r}}_T$ can be reduced and integrated while the spherical harmonics in $\hat{\mathbf{R}}$ can be written as a single spherical harmonic. Finally, the sum over $\mu$ coming from (A8) can be done yielding a Racah coefficient and the finished result,

$$\begin{aligned}
\left\langle \psi_\alpha(\mathbf{r}_T) | \phi_\beta(\mathbf{r}_P) e^{i\boldsymbol{v}_0\cdot\mathbf{r}_T} \right\rangle = {} & 4\pi^{3/2} \sum_{l_1=0}^{\infty} (-1)^{l_\beta + l_1} \sum_{l_2=|l_1-l_\beta|}^{|l_1+l_\beta|} C(l_1,l_2,l_\beta; m_\alpha, m_\beta - m_\alpha, m_\beta) Y_{l_2(m_\beta - m_\alpha)}(\hat{\mathbf{R}}) \\
& \times \sum_{l_3=|l_1-l_\alpha|}^{|l_1+l_\alpha|} i^{l_3} C(l_\alpha,l_3,l_1; m_\alpha,0,m_\alpha) C(l_\alpha,l_3,l_1;0,0,0) g(l_\alpha,l_3;l_1) \sum_{l_4=0}^{l_\beta} R^{l_\beta - l_4} f(l_\beta,l_4) \sum_{\lambda=|l_2-l_\beta+l_4|}^{|l_2+l_\beta-l_4|} \\
& \times \left[\int_0^\infty R_{n_\alpha l_\alpha}(r_T) S^\lambda_{n_\beta l_\beta}(r_T,R) j_{l_3}(v_0 r_T) r_T^{l_4+2} dr_T\right] [(2l_1+1)(2l_2+1)(2l_3+1)]^{1/2} g(l_4,\lambda;l_1) \\
& \times g(\lambda,l_\beta - l_4;l_2) C(l_4,\lambda,l_1 : 0,0,0) C(\lambda,l_\beta - l_4,l_2;0,0,0) W(l_1,\lambda,l_\beta,l_\beta - l_4;l_4,l_2),
\end{aligned} \tag{A12}$$

where $W(l_1,l_2,l_3,l_4;l_5,l_6)$ is a Racah coefficient as defined by Rose [48]. In practice the sum over $l_1$ is truncated to a finite range adequate for convergence.

The matrix elements

$$\langle\psi_\alpha(\mathbf{r}_T)|e^{i\mathbf{v}_0\cdot\mathbf{r}_T}(H-E_\beta)\phi_\beta(\mathbf{r}_P)\rangle \tag{A13}$$

and

$$\langle(H-\epsilon_\alpha)\psi_\alpha(\mathbf{r}_T)|e^{i\mathbf{v}_0\cdot\mathbf{r}_T}\phi_\beta(\mathbf{r}_P)\rangle \tag{A14}$$

required in (14) and (15) may be obtained by replacing $R_{n_\alpha l_\alpha}(r_T)S^\lambda_{n_\beta l_\beta}(r_T,R)$ in (A12) by

$$R_{n_\alpha l_\alpha}(r_T)\left(T^\lambda_{n_\beta l_\beta}(r_T,R)+\left(\frac{Z_PZ_T}{R}-\frac{Z_T}{r_T}\right)S^\lambda_{n_\beta l_\beta}(r_T,R)\right) \tag{A15}$$

and

$$U_{n_\alpha l_\alpha}(r_T)S^\lambda_{n_\beta l_\beta}(r_T,R)+R_{n_\alpha l_\alpha}(r_T)\left(\frac{Z_PZ_T}{R}S^\lambda_{n_\beta l_\beta}(r_T,R)-Z_PW^\lambda_{n_\beta l_\beta}(r_T,R)\right), \tag{A16}$$

respectively. Here $T^\lambda_{n_\beta l_\beta}$ and $W^\lambda_{n_\beta l_\beta}$ are the analogs of (A6) but with $S_{n_\beta l_\beta}(r_P)$ replaced by $T_{n_\beta l_\beta}(r_P)$ and $S_{n_\beta l_\beta}(r_P)/r_P$, respectively. $T_{n_\beta l_\beta}(r_P)$ and $U_{n_\alpha l_\alpha}(r_T)$ are defined by

$$(H_P-E_\beta)\phi_\beta(\mathbf{r}_P)\equiv T_{n_\beta l_\beta}(r_P)Y_{l_\beta m_\beta}(\hat{\mathbf{r}}_P), \tag{A17}$$

$$(H_T-\epsilon_\alpha)\psi_\alpha(\mathbf{r}_T)\equiv U_{n_\alpha l_\alpha}(r_T)Y_{l_\alpha m_\alpha}(\hat{\mathbf{r}}_T). \tag{A18}$$

For eigenstates $T_{n_\beta l_\beta}$ and $U_{n_\alpha l_\alpha}$ are identically zero, but not so for pseudostates.

The symmetries (21) and (22) follow from (A12) on realizing that the azimuthal angle of $\mathbf{R}$ is the same as that of $\mathbf{b}$. Then [48]

$$Y_{l_2(m_\beta-m_\alpha)}(\hat{\mathbf{R}})=e^{i(m_\beta-m_\alpha)\phi_b}P_{l_2(m_\beta-m_\alpha)}(\theta_R),$$
$$\cos\theta_R=v_0t/\sqrt{b^2+v_0^2t^2}\quad[\text{see (1)}], \tag{A19}$$

where $P_{lm}(\theta)$ is an associated Legendre function. The symmetry (26) follows from [48]

$$P_{l_2(-m_\beta+m_\alpha)}(\theta_R)=(-1)^{m_\beta-m_\alpha}P_{l_2(m_\beta-m_\alpha)}(\theta_R) \tag{A20}$$

and

$$C(l_1,l_2,l_3;m_1,m_2,m_3)=(-1)^{l_1+l_2-l_3}C(l_1,l_2,l_3;-m_1,-m_2,-m_3). \tag{A21}$$

Note that if $m_1=m_2=m_3=0$, (A21) implies that $l_1+l_2+l_3$ is even; this is also needed to establish (26).


[1] T. Vajnai, A. D. Gaus, J. A. Brand, W. Htwe, D. H. Madison, R. E. Olson, J. L. Peacher, and M. Schulz, Phys. Rev. Lett. **74**, 3588 (1995).

[2] M. Schulz, T. Vajnai, A. D. Gaus, W. Htwe, D. H. Madison, and R. E. Olson, Phys. Rev. A **54**, 2951 (1996).

[3] W. Schmitt, R. Moshammer, F. S. C. O'Rourke, H. Kollmus, L. Sarkadi, R. Mann, S. Hagmann, R. E. Olson, and J. Ullrich, Phys. Rev. Lett. **81**, 4337 (1998).

[4] L. C. Tribedi, P. Richard, Y. D. Wang, C. D. Lin, L. Gulyás, and M. E. Rudd, Phys. Rev. A **58**, 3619 (1998).

[5] R. Moshammer, P. D. Fainstein, M. Schulz, W. Schmitt, H. Kollmus, R. Mann, S. Hagmann, and J. Ullrich, Phys. Rev. Lett. **83**, 4721 (1999).

[6] R. Moshammer, A. N. Perumal, M. Schulz, V. D. Rodriguez, H. Kollmus, R. Mann, S. Hagmann, and J. Ullrich, Phys. Rev. Lett. **87**, 223201 (2001).

[7] M. Schulz, R. Moshammer, D. Fischer, and J. Ullrich, J. Phys. B **37**, 4055 (2004).

[8] D. Fischer, D. Globig, J. Goullon, M. Grieser, R. Hubele, V. L. B. de Jesus, A. Kelkar, A. LaForge, H. Lindenblatt, D. Misra, B. Najjari, K. Schneider, M. Schulz, M. Sell, and X. Wang, Phys. Rev. Lett. **109**, 113202 (2012).

[9] A. C. LaForge, R. Hubele, J. Goullon, X. Wang, K. Schneider, V. L. B. de Jesus, B. Najjari, A. B. Voitkiv, M. Grieser, M. Schulz, and D. Fischer, J. Phys. B **46**, 031001 (2013).

[10] M. D. Śpiewanowski, L. Gulyás, M. Horbatsch, J. Goullon, N. Ferreira, R. Hubele, V. L. B. de Jesus, H. Lindenblatt, K. Schneider, M. Schulz, M. Schuricke, Z. Song, S. Zhang, D. Fischer, and T. Kirchner, J. Phys. Conf. Ser. **601**, 012010 (2015).

[11] D. H. Madison, M. Schulz, S. Jones, M. Foster, R. Moshammer, and J. Ullrich, J. Phys. B **35**, 3297 (2002).

[12] M. Schulz, R. Moshammer, D. Fischer, H. Kollmus, D. H. Madison, S. Jones, and J. Ullrich, Nature (London) **422**, 48 (2003).

[13] D. Fischer, R. Moshammer, M. Schulz, A. Voitkiv, and J. Ullrich, J. Phys. B **36**, 3555 (2003).

[14] M. Schulz, R. Moshammer, D. Fischer, and J. Ullrich, J. Phys. B **36**, L311 (2003).

[15] A. B. Voitkiv, B. Najjari, R. Moshammer, M. Schulz, and J. Ullrich, J. Phys. B **37**, L365 (2004).

[16] N. V. Maydanyuk, A. Hasan, M. Foster, B. Tooke, E. Nanni, D. H. Madison, and M. Schulz, Phys. Rev. Lett. **94**, 243201 (2005).

[17] M. Schulz, R. Moshammer, A. Voitkiv, B. Najjari, and J. Ullrich, Nucl. Instrum. Methods Phys. Res. Sect. B **235**, 296 (2005).

[18] A. C. Laforge, K. N. Egodapitiya, J. S. Alexander, A. Hasan, M. F. Ciappina, M. A. Khakoo, and M. Schulz, Phys. Rev. Lett. **103**, 053201 (2009).

[19] M. Schulz, A. C. Laforge, K. N. Egodapitiya, J. S. Alexander, A. Hasan, M. F. Ciappina, A. C. Roy, R. Dey, A. Samolov, and A. L. Godunov, Phys. Rev. A **81**, 052705 (2010).

[20] R. Hubele, A. LaForge, M. Schulz, J. Goullon, X. Wang, B. Najjari, N. Ferreira, M. Grieser, V. L. B. de Jesus, R. Moshammer, K. Schneider, A. B. Voitkiv, and D. Fischer, Phys. Rev. Lett. **110**, 133201 (2013).

[21] M. McGovern, D. Assafrão, J. R. Mohallem, Colm T. Whelan, and H. R. J. Walters, Phys. Rev. A **79**, 042707 (2009).

[22] M. McGovern, D. Assafrão, J. R. Mohallem, C. T. Whelan, and H. R. J. Walters, J. Phys. Conf. Ser. **194**, 012042 (2009).

[23] M. McGovern, D. Assafrão, J. R. Mohallem, C. T. Whelan, and H. R. J. Walters, J. Phys. Conf. Ser. **212**, 012029 (2010).

[24] M. McGovern, H. R. J. Walters, and C. T. Whelan, in *Fragmentation Processes*, edited by C. T. Whelan (Cambridge University Press, Cambridge, U.K., 2013), p. 155.

[25] M. McGovern, D. Assafrão, J. R. Mohallem, Colm T. Whelan, and H. R. J. Walters, Phys. Rev. A **81**, 032708 (2010).

[26] M. McGovern, D. Assafrão, J. R. Mohallem, C. T. Whelan, and H. R. J. Walters, Phys. Rev. A **81**, 042704 (2010).

[27] M. McGovern, C. T. Whelan, and H. R. J. Walters, Phys. Rev. A **82**, 032702 (2010).

[28] H. R. J. Walters and C. T. Whelan, Phys. Rev. A **89**, 032709 (2014).

[29] M. E. Rudd, C. A. Sautter, and C. L. Bailey, Phys. Rev. **161**, 1 (1967).

[30] J. Macek, Phys. Rev. A **1**, 235 (1970).

[31] This work was earlier reported at the ISIAC conference in Caen, France, in 2011.

[32] E. P. Curran and H. R. J. Walters, J. Phys. B **20**, 337 (1987).

[33] E. P. Curran and H. R. J. Walters, J. Phys. B **20**, 1105 (1987).

[34] T. G. Winter, Phys. Rev. A **80**, 032701 (2009).

[35] We note that, in regard to the factor $e^{i\mathbf{q}\cdot\mathbf{R}}$, (33) has exactly the same structure as for a nonexchange transition; i.e., $f_{f0}^{B1} = -\frac{1}{2\pi}\int e^{i\mathbf{q}\cdot\mathbf{R}}\langle\psi_f(\mathbf{r}_T)|V_T|\psi_0(\mathbf{r}_T)\rangle d\mathbf{R}$. This is an important point when it comes to the iterative solutions of the equations of [37] leading to the impact-parameter-wave relationship (40); see [21].

[36] For the elastic channel $f = 0$ we need to subtract out the starting value (38); see [21].

[37] The corresponding wave version of (6) is

$$\Psi = \sum_{\alpha=1}^{N} F_\alpha(\mathbf{R}_P)\psi_\alpha(\mathbf{r}_T) + \sum_{\beta=1}^{M} G_\beta(\mathbf{R}_{Pe})\phi_\beta(\mathbf{r}_P),$$

leading to the coupled equations

$$\begin{aligned}
\left(\nabla_{R_P}^2 + k_\alpha^2\right)F_\alpha(\mathbf{R}_P) &= 2\mu_P\sum_{\alpha'=1}^{N}\langle\psi_\alpha(\mathbf{r}_T)|V_T|\psi_{\alpha'}(\mathbf{r}_T)\rangle F_{\alpha'}(\mathbf{R}_P) \\
&\quad + 2\mu_P\sum_{\beta=1}^{M}\langle\psi_\alpha(\mathbf{r}_T)|(H-E)| \\
&\quad \times G_\beta(\mathbf{R}_{Pe})\phi_\beta(\mathbf{r}_P)\rangle, \\
\left(\nabla_{R_{Pe}}^2 + k_\beta^2\right)G_\beta(\mathbf{R}_{Pe}) &= 2\mu_{Pe}\sum_{\beta'=1}^{M}\langle\phi_\beta(\mathbf{r}_P)|V_P|\phi_{\beta'}(\mathbf{r}_P)\rangle G_{\beta'}(\mathbf{R}_{Pe}) \\
&\quad + 2\mu_{Pe}\sum_{\alpha=1}^{N}\langle\phi_\beta(\mathbf{r}_P)|(H-E) \\
&\quad \times |F_\alpha(\mathbf{R}_P)\psi_\alpha(\mathbf{r}_T)\rangle,
\end{aligned}$$

in an obvious notation.

[38] H. R. J. Walters, X. Zhang, and C. T. Whelan, in *(e, 2e) and Related Processes*, edited by C. T. Whelan, H. R. J. Walters, A. Lahmam-Bennani, and H. Ehrhardt (Kluwer, Dordrecht, 1993), p. 33.

[39] The pseudostate amplitudes in (46) and (47) are in general off energy shell. The result (40) is technically only valid on energy shell. Here we use the relaxed form of the approximation in which this difference is ignored. This is discussed in [21,25].

[40] We use the "principal" quantum number $n$ to label the states even though they are a mixture of eigenstates and pseudostates.

[41] I. Bray and A. T. Stelbovics, Phys. Rev. A **46**, 6995 (1992).

[42] Note that, although $P \propto |f_{\rm ion}^P|^2$ may be small compared to $T \propto |f_{\rm ion}^T|^2$, the linear combination of $f_{\rm ion}^P$ with $f_{\rm ion}^T$ in CO $\propto |f_{\rm ion}^T + f_{\rm ion}^P|^2$, before squaring, can give a much greater influence.

[43] Note that the angles in Fig. 6 cover momentum transfers ranging up to 3.4 a.u. This goes well beyond the limit of $q = 1.5$ a.u. studied in Figs. 1–5. At the ejection energies of 5, 10, 16.395, 26.395, 36.395, and 39.395 eV, a momentum transfer $q = 1.5$ a.u. corresponds to laboratory proton scattering angles of 0.45, 0.44, 0.43, 0.39, 0.33, and 0.31 mrad, respectively.

[44] K. N. Egodapitiya, S. Sharma, A. Hasan, A. C. Laforge, D. H. Madison, R. Moshammer, and M. Schulz, Phys. Rev. Lett. **106**, 153202 (2011).

[45] S. Sharma, A. Hasan, K. N. Egodapitiya, T. P. Arthanayaka, G. Sakhelashvili, and M. Schulz, Phys. Rev. A **86**, 022706 (2012).

[46] X. Wang, K. Schneider, A. LaForge, A. Kelkar, M. Grieser, R. Moshammer, J. Ullrich, M. Schulz, and D. Fischer, J. Phys. B **45**, 211001 (2012).

[47] M. B. Shah, D. S. Elliott, and H. B. Gilbody, J. Phys. B **20**, 2481 (1987).

[48] M. E. Rose, *Elementary Theory of Angular Momentum* (Wiley, New York, 1957).

[49] S. Charkrabarti and D. P. Dewangan, J. Phys. B **28**, L769 (1995).